

Prediction and Measurement of the Interparticle Depletion Interaction Next to a Flat Wall

Martin Piech,^{*} Paweł Weroniński,^{*} Xin Wu,[†] and John Y. Walz^{*,1}

^{*}Yale University, Department of Chemical Engineering, P.O. Box 208286, New Haven, Connecticut 06520-8286; and [†]Synchrude Canada Ltd., Edmonton Research Centre, Edmonton, Alberta T6N 1H4, Canada

Received July 31, 2001; accepted November 24, 2001

A theoretical and experimental study was performed to investigate the depletion interaction between two colloidal particles next to a solid wall in a solution of nonadsorbing macromolecules. By calculating the change in free volume available to the macromolecules upon approach of the two particles, a relatively simple expression was developed for the interparticle depletion attraction in hard sphere systems as a function of the particle–particle and particle–plate spacing. Perhaps the most useful result obtained from this analysis was that the wall has no effect whenever the ratio of the particle radius to the macromolecule radius is greater than four. (In charged systems, this ratio would apply to the effective particle and macromolecule sizes.) A series of experiments was then performed in which the hydrodynamic force balance (HFB) apparatus was used to measure the shear force needed to separate a colloidal doublet consisting of two particles trapped in a secondary energy well formed by a repulsive electrostatic force and an attractive depletion force. The macromolecules used here were small, nanometer-sized spheres of either silica or polystyrene. Agreement between the measured separation forces and those predicted using the force balance model of J. Y. Walz and A. Sharma (*J. Colloid Interface Sci.* 168, 485 (1994)) was within a factor of 1.3 using no adjustable parameters and accounting for polydispersity and uncertainty in the macromolecule size. It is shown that this remaining discrepancy could be caused by the Brownian (stochastic) nature of the doublet breakup process. © 2002 Elsevier Science (USA)

Key Words: depletion interaction; depletion forces; polyelectrolytes; surface forces; hydrodynamic force balance technique.

INTRODUCTION

Ever since the pioneering work of Asakura and Oosawa in the 1950s (1, 2), the depletion interaction between colloidal particles immersed in a solution of nonadsorbing polymers has been the subject of a substantial amount of research. Numerous groups have demonstrated, both experimentally and computationally, that even at relatively low polymer concentrations (i.e., order 1% wt), the depletion attraction can be significant enough to introduce phase transitions in an otherwise stable colloidal dispersion (3–6). In addition, several novel and useful applications of the depletion interaction have been demonstrated. For exam-

ple, Promislow (7) showed that the depletion attraction produced by ionic micelles could be used to selectively separate different size fractions of oil-in-water emulsion droplets. Zukoski and coworkers have shown that nonadsorbing poly(ethylene glycol) can induce crystallization and/or separation of protein solutions (8–10). Finally, nonadsorbing polysaccharides are used as thickening agents in milk products, where the fundamental mechanism is believed to be a depletion attraction between casein micelles arising from the presence of the polysaccharides (11).

Another area in which depletion interactions may prove useful is in patterning particles next to an interface. Such a use of small, nonadsorbing particles to manipulate larger colloids in two-dimensional space next to a wall was demonstrated in a series of experiments by Yodh and coworkers (12–14). These authors found that the larger particles are pushed away from the edge of a downward step yet into the corner of a vertical rise (i.e., a wall meeting a floor). Each of these results could be explained using the concept that the particle will move in the direction that maximizes the free volume available to the smaller, nonadsorbing species. Dinsmore and Yodh (15) also found that the higher concentrations near vertical corners caused particle crystallites to form in these areas prior to forming either along the flat wall or in the bulk.

Before such a method can be exploited, however, a better understanding of the depletion interaction between two particles next to a wall needs to be developed. This paper presents a theoretical and experimental study of the interparticle depletion interaction between two spherical particles next to a flat, solid surface. In the theory section, an analytical equation is developed for predicting how the bulk interparticle depletion interaction is modified by the presence of the wall. Next, a series of experiments is presented in which the hydrodynamic force balance (HFB) technique was used to measure the maximum attractive force between two charged particles very close to a solid plate in a solution of nonadsorbing charged nanospheres. Because of the relative sizes of the particles and nanospheres, the depletion interaction between the two particles is predicted to be unaffected by the wall under the specific experimental conditions. Comparisons between the measured forces and those predicted using the force balance approach originally developed by Walz and Sharma (16) are also given.

¹ To whom correspondence should be addressed.

THEORY

The equation for the depletion interaction between two colloidal particles is typically derived in several different ways. For the present analysis, the procedure that works best is that considering the change in excluded volume when two particles approach each other, which is the method originally used by Asakura and Oosawa (1, 2).

At low concentrations, the net interaction force between two colloidal particles immersed in a solution of nonadsorbing macromolecules (see Fig. 1) will be given by (1)

$$F = kTN \frac{\partial \ln Q}{\partial h}, \quad [1]$$

where

$$Q = \int_{\mathbf{x}} \exp\left[-\frac{w(\mathbf{x})}{kT}\right] d\mathbf{x}. \quad [2]$$

Here kT is thermal energy, N is the total number of macromolecules in the system, h is the gap width between the two particles, and $w(\mathbf{x})$ is the free energy of a macromolecule located at position \mathbf{x} . The integral in Eq. [2] is over the entire system volume. For the case of purely hard particles and macromolecules (i.e., only hard wall interactions), Q will be given by the total free volume available to the macromolecules and Eq. [1] can be written as

$$F = kT(N/V_{\text{free}}) \frac{\partial V_{\text{free}}}{\partial h}. \quad [3]$$

When the volume fraction of particles and macromolecules is relatively small, the term N/V_{free} will be approximately equal to the bulk number density of macromolecules, ρ_{∞} . Since the

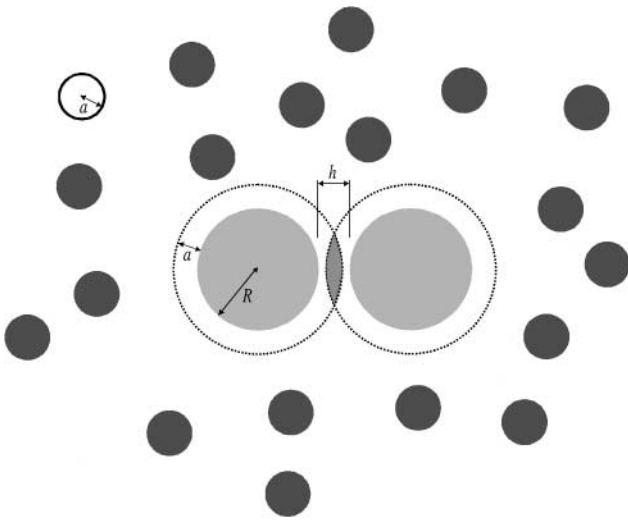


FIG. 1. This schematic shows the origin of the depletion interaction between two particles of radius R in the bulk. Each particle excludes macromolecules of radius a , from a spherical volume of radius $R + a$. When these exclusion volumes overlap, the total free volume available to the macromolecules is increased, which is energetically favorable.

total volume of the system is assumed fixed, the depletion force can be calculated as

$$F = -kT\rho_{\infty} \frac{\partial V_{\text{excl}}}{\partial h}, \quad [4]$$

where V_{excl} is the volume of the system excluded from the macromolecules ($V_{\text{excl}} = V_{\text{total}} - V_{\text{free}}$). Here, a negative value of the force implies an attraction between the particles. The depletion attraction arises when the total excluded volume of the system decreases with decreasing gap width, which is energetically favorable in a purely hard sphere system.

Consider first the case of two spherical particles of radius R , separated by gap width h , immersed in a solution of hard, spherical macromolecules of radius a (see Fig. 1). Each isolated particle excludes a spherical volume of radius $(R + a)$ from the macromolecules. When the particles approach sufficiently close, however, these two excluded volumes overlap by the volume of the shaded region in this figure, $V_{\text{particle-particle}}^{\text{overlap}}$, and the total excluded volume of the system actually decreases by this amount. The depletion force can now be calculated as

$$F_{\text{particle-particle}} = +kT\rho_{\infty} \frac{\partial (V_{\text{particle-particle}}^{\text{overlap}})}{\partial h}. \quad [5]$$

Through simple geometry, the volume of this overlap region can be shown to equal

$$V_{\text{particle-particle}}^{\text{overlap}} = \begin{cases} \frac{2}{3}\pi(a - \frac{h}{2})^2(3R + 2a + \frac{h}{2}) & \text{for } h < 2a \\ 0 & \text{for } h \geq 2a. \end{cases} \quad [6]$$

Substituting Eq. [6] into Eq. [5] and differentiating with respect to h yields

$$\frac{F_{\text{particle-particle}}(h)}{\rho_{\infty}kT\pi aR} = \begin{cases} -(2 + \frac{a}{R} - \frac{h}{a} - \frac{h^2}{4aR}) & \text{for } 0 \leq h < 2a \\ 0 & \text{for } h \geq 2a, \end{cases} \quad [7]$$

which is the classical Asakura and Oosawa expression for the depletion force between two spherical particles (1).

A similar approach can be used to calculate the depletion interaction between a single particle and a flat plate, shown in Fig. 2. Now the depletion force will be given by

$$F_{\text{particle-plate}} = +kT\rho_{\infty} \frac{\partial (V_{\text{particle-plate}}^{\text{overlap}})}{\partial h'}, \quad [8]$$

where h' is the particle-plate gap width and $V_{\text{particle-plate}}^{\text{overlap}}$ (the shaded region in Fig. 2) is given by

$$V_{\text{particle-plate}}^{\text{overlap}} = \begin{cases} \frac{\pi}{3}(2a - h')^2(3R + a + h') & \text{for } h' < 2a \\ 0 & \text{for } h' \geq 2a. \end{cases} \quad [9]$$

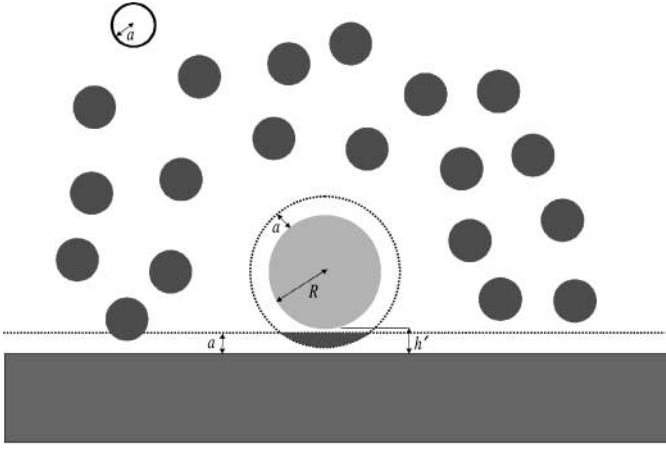


FIG. 2. This schematic shows the origin of the depletion interaction between a spherical particle and a flat wall. The spherical macromolecules are excluded from a region of thickness a around the particle and also next to the wall. The overlap of these excluded volume regions (indicated by the shaded region) is energetically favorable, producing an attraction between the particle and wall.

Combining Eqs. [8] and [9] yields

$$\frac{F_{\text{particle-plate}}}{\rho_{\infty} kT \pi a R} = \begin{cases} -(4 + 2\frac{h'}{R} - 2\frac{h'}{a} - \frac{(h')^2}{aR}) & \text{for } h' < 2a \\ 0 & \text{for } h' \geq 2a, \end{cases} \quad [10]$$

which is approximately twice the particle–particle interaction for $R \gg a$ (i.e., the Derjaguin limit).

Now consider the situation depicted in Fig. 3, in which two particles are interacting simultaneously with each other and a neighboring wall. The issue is whether the particle–particle and

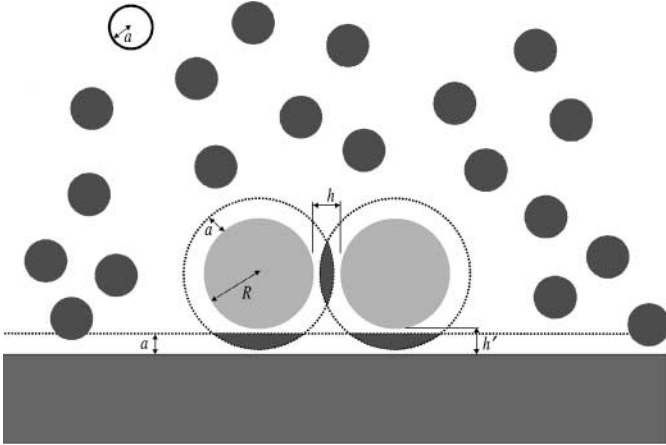


FIG. 3. This schematic shows a situation in which two particles experience a depletion interaction between themselves and between a neighboring wall. However, because the overlapping particle–particle and particle–wall excluded volumes (shaded areas) do not overlap with each other, the particle–particle and particle–wall depletion interactions can be calculated independently using Eqs. [7] and [10].

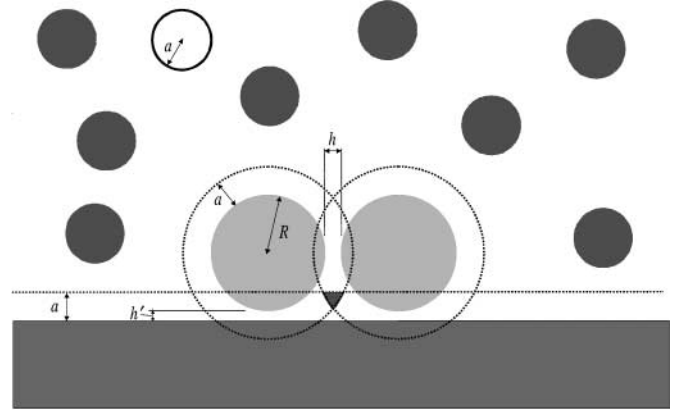


FIG. 4. This figure illustrates the case when the particle–particle and particle–wall excluded volume regions mutually overlap. The necessary correction to Eqs. [6] and [9] is equal to the volume of the small shaded region. Note that the relative sizes of the particles and macromolecules have been changed in this figure compared to Fig. 3 simply for illustration purposes.

particle–wall interactions can be calculated independently using Eqs. [7] and [10] above or whether there is, in fact, some coupling between the two interactions. This coupling can be seen clearly in the simple schematics presented in Figs. 3 and 4. In Fig. 3, the overlaps of the excluded volumes are clearly independent of each other, meaning that the interactions can be calculated separately. In other words, small changes in the interparticle gap width would only affect the interparticle overlap region. Likewise, small changes in the particle–wall gap width would only affect the two particle–wall overlap regions.

On the other hand, Fig. 4 presents a system in which the particle–particle and particle–wall overlap regions mutually overlap by the amount indicated by the shaded region. Now the total volume of the overlapping excluded volume regions will be given by the particle–particle overlap volume, $V_{\text{particle-particle}}^{\text{overlap}}$, plus twice the single particle–plate overlap volume, $V_{\text{particle-plate}}^{\text{overlap}}$, minus the shared overlap volume, $V_{\text{shared}}^{\text{overlap}}$, shown as the shaded region in Fig. 4. Thus according to Eq. [4], the particle–particle depletion force will be given by

$$F_{\text{particle-particle}} = +kT\rho_{\infty} \frac{\partial (V_{\text{particle-particle}}^{\text{overlap}} + 2V_{\text{particle-plate}}^{\text{overlap}} - V_{\text{shared}}^{\text{overlap}})}{\partial h}. \quad [11]$$

(Note that $V_{\text{particle-plate}}^{\text{overlap}}$ has been multiplied by a factor of 2 here because two particles are present.) The volume of the shared overlap region indicated in Fig. 4 is given by

$$V_{\text{shared}}^{\text{overlap}} = 2 \int_{x_0}^{x_m} \left[\frac{\pi}{2} (\bar{R}^2 - x^2) - (\bar{R}^2 - x_m^2)^{1/2} (x_m^2 - x^2)^{1/2} + (x^2 - \bar{R}^2) \sin^{-1} \left(\frac{\bar{R}^2 - x_m^2}{\bar{R}^2 - x^2} \right)^{1/2} \right] dx, \quad [12]$$

where $\bar{R} = (R + a)$, $x_0 = R + (h/2)$, and $x_m = [4aR - h'(h' + 2R + 2a)]^{1/2}$. The meanings of x_0 and x_m , as well as the limits over which Eq. [12] applies, can be seen in the schematic shown in Fig. 5, which is an expanded view of the region of mutual overlap. The volume, $V_{\text{shared}}^{\text{overlap}}$, given by Eq. [12] is twice the volume of the shaded region. As seen, this volume becomes zero when x_0 and x_m become equal. From the definitions of x_0 and x_m , this can be shown to occur when

$$\left(R + \frac{h}{2}\right)^2 + h'(h' + 2R + 2a) \geq 4aR. \quad [13]$$

The derivative of $V_{\text{particle-particle}}^{\text{overlap}}$ with respect to h in Eq. [11] simply leads to the bulk particle-particle depletion attraction given by Eq. [7]. Because $V_{\text{particle-plate}}^{\text{overlap}}$ is independent of h , the derivative of this term with respect to h is zero. Thus the correction to the bulk particle-particle depletion attraction required by the presence of the wall will be given by the derivative of Eq. [12] with respect to h . As seen from the definitions of x_0 and x_m , h appears only in the lower limit of the integral in this equation. Thus using the chain rule of derivatives, we can write

$$\begin{aligned} \frac{\partial V_{\text{shared}}^{\text{overlap}}}{\partial h} &= \frac{\partial V_{\text{shared}}^{\text{overlap}}}{\partial x_0} \frac{\partial x_0}{\partial h} = -2f_{\text{integrand}}(x = x_0) \left(\frac{1}{2}\right) \\ &= -f_{\text{integrand}}(x = x_0), \end{aligned} \quad [14]$$

where $f_{\text{integrand}}(x)$ is the integrand in Eq. [12]. Thus

$$\frac{\partial V_{\text{shared}}^{\text{overlap}}}{\partial h} = \begin{cases} -\left[\frac{\pi}{2} [\bar{R}^2 - x_0^2] - (\bar{R}^2 - x_m^2)^{1/2} (x_m^2 - x_0^2)^{1/2} \right. \\ \quad \left. + (x_0^2 - \bar{R}^2) \sin^{-1} \left(\frac{\bar{R}^2 - x_m^2}{\bar{R}^2 - x_0^2} \right)^{1/2} \right] & \text{for } \left(R + \frac{h}{2}\right)^2 + h'(h' + 2R + 2a) < 4aR \\ 0 & \text{for } \left(R + \frac{h}{2}\right)^2 + h'(h' + 2R + 2a) \geq 4aR. \end{cases} \quad [15]$$

The complete expression for the interparticle depletion force next to a wall can be written

$$\begin{aligned} \frac{F_{\text{particle-particle}}(h)}{\rho_{\infty} kT \pi a R} &= \begin{cases} -(2 + \frac{a}{R} - \frac{h}{a} - \frac{h^2}{4aR}) & \text{for } 0 \leq h < 2a \\ 0 & \text{for } h \geq 2a \end{cases} \\ &+ \frac{1}{\pi a R} \begin{cases} \left[\frac{\pi}{2} (\bar{R}^2 - x_0^2) - (\bar{R}^2 - x_m^2)^{1/2} (x_m^2 - x_0^2)^{1/2} \right. \\ \quad \left. + (x_0^2 - \bar{R}^2) \sin^{-1} \left(\frac{\bar{R}^2 - x_m^2}{\bar{R}^2 - x_0^2} \right)^{1/2} \right] & \text{for } \left(R + \frac{h}{2}\right)^2 + h'(h' + 2R + 2a) < 4aR \\ 0 & \text{for } \left(R + \frac{h}{2}\right)^2 + h'(h' + 2R + 2a) \geq 4aR \end{cases}. \end{aligned} \quad [16]$$

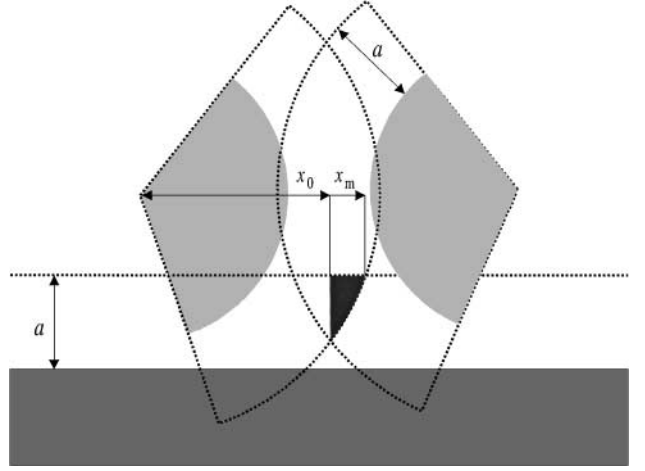


FIG. 5. This schematic shows an expanded view of the shared particle-particle and particle-plate overlap regions, $V_{\text{shared}}^{\text{overlap}}$. The value of $V_{\text{shared}}^{\text{overlap}}$ will be twice that of the shaded region and will become zero when x_0 equals x_m . (Note that both x_0 and x_m are measured from the particle center.)

Note that the second term on the rhs of Eq. [16] will be zero whenever the first term is zero (i.e., whenever $h \geq 2a$).

It is interesting to examine how the correction to the bulk particle-particle interaction in Eq. [16] depends on the ratio of the macromolecule size to the particle size, a/R . For this analysis, we will use the maximum possible value of the correction (Eq. [15]), which occurs when both h and h' equal zero (i.e., the particles are in physical contact with each other and the wall). Under these conditions, the limits given in Eq. [13] reduce to simply $R \geq 4a$. In other words, for systems in which

the particle size is at least four times the macromolecule size, the wall effects will always be zero and the interparticle depletion interaction can be calculated using Eq. [7].

Although the approach described here is restricted to the case of purely hard sphere systems where interactions are completely entropic in nature, Piech and Walz [17] showed that the depletion interaction in charged systems can also be calculated using this method provided that the actual macromolecule size is replaced by an effective size that takes into account the thickness of the charged double layer around the particles and macromolecules. The authors presented an approximate formula for calculating the effective double-layer thickness, but found that for typical surface potentials in aqueous systems, this thickness was roughly equal to five times the bulk Debye length, or $5\kappa^{-1}$. This value was also observed in experimental measurements of the depletion interaction by Odiachi and Prieve [18]. Using this criterion, we can state that wall effects are negligible in systems where $R \geq 4(a + 5\kappa^{-1})$.

EXPERIMENTAL

Overview of Technique

Measurements of the depletion interaction between two colloidal particles next to a solid plate were made with the hydrodynamic force balance (HFB) apparatus located at the Syncrude Research Centre in Edmonton, Alberta. A brief overview of the technique will be presented here; more details can be found in Wu *et al.* (19).

A simplified schematic of the HFB technique is shown in Fig. 6. In the experiments, the drag force produced by a linear shear flow is used to separate two identical colloidal particles

that have been brought into direct contact. One of the particles is actually adhered to a solid, stationary plate and remains fixed in position during the shear flow. The second particle is held very close to the plate by gravitational (buoyancy) forces yet can still translate in the shear flow.

The hydrodynamic force acting on the free particle will be a function of its distance from both the wall and the neighboring particle. Following the notation of Wu *et al.*, we let y_b represent the dimensionless distance (normalized by the particle radius) between the centers of the free particle and the fixed particle, while z_b represents the dimensionless distance between the center of the free particle and the wall. If we assume that a line segment connecting the two particle centers is parallel to the flow direction, then the force on the free particle normal to the direction of flow (the x -direction in Fig. 6) will be zero. As pointed out by Wu *et al.*, if the two particles are slightly out of alignment, the drag force in the x -direction will simply tend to align them prior to breakup.

Dabros and van de Ven (20) solved the Stokes and continuity equations to obtain the net drag force exerted on the free particle. Using this solution, Wu *et al.* found that when the dimensionless distance between the two particles, y_b , was less than approximately 2.04 (i.e., a gap width less than $0.04R$), the drag force in the direction of flow was essentially independent of y_b . In the particular experiments described here (see details below), $0.04R$ corresponds to a gap width of approximately 200 nm. Since this is beyond the typical range of colloidal interactions, we assume here that the drag force acting on the particle will depend only on the distance between the free particle and plate.

At particle breakup, the net colloidal force between the particles will be just balanced by the vector sum of the drag and net

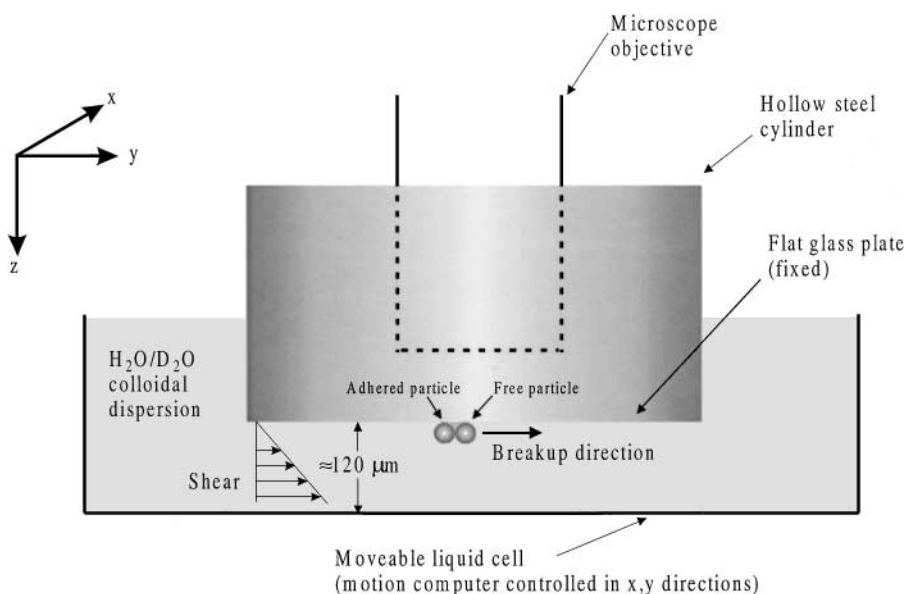


FIG. 6. This schematic shows an expanded view of the HFB apparatus in the region of the colloidal doublet. The liquid cell is translated at a controlled velocity, creating a linear shear flow in the gap region. At a sufficiently high shear rate, the free particle in the doublet will separate from the adhered particle.

gravitational forces (buoyancy). Thus

$$F_{\text{coll}} = F_{\text{drag},y}(z_b) \frac{y_b}{\sqrt{y_b^2 + (z_b - 1)^2}} + F_z \frac{z_b - 1}{\sqrt{y_b^2 + (z_b - 1)^2}}, \quad [17]$$

where F_{coll} is the colloidal force, $F_{\text{drag},y}(z_b)$ is the drag force, and F_z is the force in the z -direction (normal to the plate), which is composed of $F_{\text{drag},z}$ and gravity. In the experiments described here, the free particle is assumed to be in an equilibrium position next to the plate; thus, the net force normal to the plate will be zero. For values of z_b between 1.01 and 2.0, Wu *et al.* found that $F_{\text{drag},y}$ could be accurately approximated by the linear relationship

$$F_{\text{drag},y} \approx 6\pi\mu GR^2[1.16 + 1.19(z_b - 1)], \quad [18]$$

where μ is the fluid viscosity and G is the linear shear rate. For values of z_b less than approximately 1.01, the term in brackets on the rhs of Eq. [18] is approximately 1.17 and F_{coll} becomes approximately the same as $F_{\text{drag},y}$. Combining Eqs. [17] and [18] under this condition yields

$$F_{\text{coll}} \approx 1.17(6\pi\mu GR^2). \quad [19]$$

In the experiments described below, z_b equal to 1.01 corresponds to a particle–plate gap width of approximately 50 nm. Although the actual gap widths in the experiments are probably slightly greater than this (perhaps as large as 100 nm), the inaccuracy in-

roduced is still relatively small (i.e., less than a few percent) and certainly less than the uncertainty present in some of the other measured parameters (see Discussion below). Thus Eq. [19] was deemed suitable for analyzing the experimental results.

It should be emphasized that this experiment yields one point on the force profile curve, namely the point of maximum attraction (excluding the actual force of adhesion). However, this force is clearly of great importance, as it determines the strength of the aggregates formed in the secondary depletion flocculation process.

Description of HFB Apparatus

The sample cell in the HFB apparatus consisted of two parts (see Fig. 7). The lower part was an open-top square box with a mirrored glass bottom. The particle solution was poured into this box to a depth of several millimeters. The second part of the cell was a stainless steel, cylindrical tube (5 cm diameter) with a smooth glass plate glued to the bottom. This tube was lowered into the sample solution such that the glass plate was approximately 120 μm above the glass bottom of the box. A microscope objective (Zeiss LD-Achroplan, 32x, 0.4 NA) was then lowered into the top of the tube such that it could be focused to any point in the fluid between the two glass plates. The actual gap width was determined by focusing on both the top and the bottom plates and then measuring the height difference using an electronic displacement transducer (Omega Engineering). The orientation of the top glass plate was controlled using tilt stages such that the gap spacing was uniform across the plates.

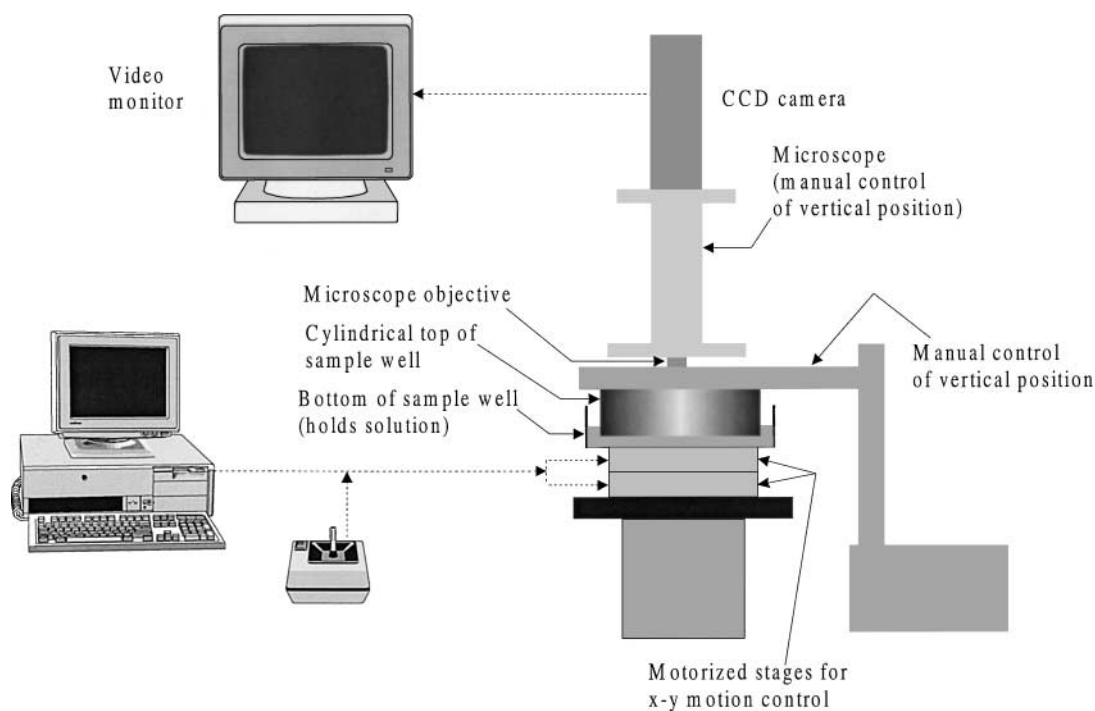


FIG. 7. This schematic shows an overview of the complete HFB apparatus. The x - y position of the sample well is computer controlled via a motion control program, and the doublet breakup process can be viewed via a CCD camera and a video monitor.

The density of the particle solution was controlled to 1.07 using an H₂O/D₂O mixture. In this manner, the large polystyrene latex particles used in the experiments (sp gr = 1.05) floated up against the top glass plate until the electrostatic repulsion between the negatively charged particles and plate was balanced by gravitational (buoyancy) and depletion forces (van der Waals forces between the particles and plate were calculated to be relatively weak).

The bottom, square box rested on two stacked, motor-controlled translation stages that allowed moving the box in both the *x* and the *y* directions. A motion-control computer program with a joystick interface was used to accurately control the position of these stages, which set the position of the bottom box. In addition, this program could be used to drive either one of the stages (*x* or *y* directions) at a set velocity. Since the gap width between the two plates was known, the shear rate in the gap could be easily calculated. Because the size of both plates was orders of magnitude greater than the gap width, edge effects could be safely ignored.

Experimental Materials

Water for preparing the solutions was produced using a MilliQ deionization system from Millipore equipped with a 0.22- μ m filter. The measured resistivity was always at least 18.2 M Ω -cm. D₂O was obtained from Aldrich as 99.9% D and was used as purchased. Reagent-grade KCl was purchased from Sigma and was used without further purification. For each solution, the relative proportion of H₂O (sp gr = 0.996) and D₂O (sp gr = 1.107) was varied to give a target solution density of 1.07. The specific conditions used in the experiments are listed in Table 1.

Monodisperse sulfate polystyrene latex spheres of mean diameter $9.6 \pm 0.7 \mu\text{m}$ were purchased from Interfacial Dynamics Corporation (Portland, OR) as a dispersion in distilled, deionized water. These particles were washed by several cycles of sedimentation/redispersion followed by a purified nitrogen purge until the styrene odor was removed. Zeta potentials of the particles were measured at varying electrolyte and hydronium ion concentrations using a microelectrophoresis apparatus (model MKII, Rank Brothers, Ltd., Cambridge, England). Care was taken to perform the zeta potential measurements at the same ionic strength and pH values as those used in the HFB experiments. The measurement results are reported in Table 1.

Three different types of particles were utilized as macromolecules. Sulfate polystyrene latex spheres with mean diameters 21 ± 3 and 38 ± 5 nm were purchased from Interfacial Dynamics Corporation (Portland, OR) as a 7.77 vol% dispersion in distilled, deionized water. These particles were dialyzed by the manufacturer and contained H⁺ as the counterion. Ludox grade AM-30 colloidal silica was obtained from Aldrich Chemical Company (Milwaukee, WI) as a 30 wt% aqueous dispersion. These macromolecules were charge stabilized with Na⁺ as the counterion. All macromolecules used in the experiments were dialyzed against deionized water (resistivity at least 18.2 M Ω -cm) for a period of 2 weeks with the water changed every day. In the case of polystyrene macromolecules, sizes were checked with transmission electron microscopy (TEM) and photon correlation spectroscopy (PCS). A Brookhaven ZetaPlus instrument (Brookhaven Instruments Corporation, Holtsville, NY) with multiangle sizing option was used for the PCS analysis. The results of these measurements are summarized in Table 1.

TABLE 1
Summary of the Experimental Conditions Used in Each of the HFB Experiments

Expt No.	Polystyrene particle diameter (μm)	Macromolecule			Concentration of indifferent electrolyte (mM)	Effective ionic strength ^b (mM)	pH	Particle zeta potential ^c (mV)	Macro. zeta potential ^c (mV)	Suspension viscosity (22°C) ^d (cP)
		Material	Manufacturer's reported diameter (nm)	Measured diameter ^a (nm)						
1	9.6 ± 0.7	Silica	12 ^e	—	0.05	0.384	6.15	-56 ± 11	-42 ± 9	1.09
2	9.6 ± 0.7	Silica	12 ^e	—	0.50	0.386	6.50	-54 ± 11	-42 ± 9	1.19
3	9.6 ± 0.7	Silica	12 ^e	—	0.50	0.923	1.14	-46 ± 10	-37 ± 10	1.19
4	9.6 ± 0.7	Silica	12 ^e	—	0.50	1.45	1.67	-39 ± 11	-33 ± 13	1.13
5	9.6 ± 0.7	Silica	12 ^e	—	0.80	0.389	6.51	-52 ± 9.5	-41 ± 10	1.20
6	9.6 ± 0.7	PS latex	21 ± 3	22.5 ± 3.8	0.05	0.387	4.28	-56 ± 9.0	-54 ± 10	1.11
7	9.6 ± 0.7	PS latex	21 ± 3	22.5 ± 3.8	0.25	0.364	3.78	-53 ± 8.5	-54 ± 8	1.13
8	9.6 ± 0.7	PS latex	21 ± 3	22.5 ± 3.8	0.50	0.386	3.57	-49 ± 8.0	-52 ± 9	1.17
9	9.6 ± 0.7	PS latex	21 ± 3	22.5 ± 3.8	0.68	0.387	3.47	-42 ± 7.0	-49 ± 7	1.18
10	9.6 ± 0.7	PS latex	38 ± 5	54.7 ± 10.4	0.006	0.386	5.44	-57 ± 11	-58 ± 7	1.11
11	9.6 ± 0.7	PS latex	38 ± 5	54.7 ± 10.4	0.05	0.387	4.79	-56 ± 11	-58 ± 7	1.11
12	9.6 ± 0.7	PS latex	38 ± 5	54.7 ± 10.4	0.05	1.45	4.79	-43 ± 9.0	-66 ± 7	1.11

^a Measured using dynamic light scattering.

^b Includes counterions released from macromolecules.

^c Measured using electrophoresis.

^d Measured using a Canon-Fenske viscometer.

^e Obtained from a Dupont data sheet on Ludox colloidal silica.

As can be seen, the measured size of the smaller polystyrene particles agrees very well with the manufacturer specifications. However, the size of the larger polystyrene particles measured by both TEM and PCS was significantly larger than value quoted by the manufacturer. The Ludox AM-30 macromolecules could not be reliably characterized by either of the two techniques because of poor contrast and low repeatability.

To estimate macromolecule valence, simultaneous conductivity and pH measurements were performed on samples of increasing macromolecule concentration (determined by evaporating water from a sample and measuring the weight loss). These measurements were performed with solutions having different background electrolyte concentrations to check the dependence of macromolecule valence on the solution ionic strength. In the case of polystyrene latexes, this analysis determined H^+ to be the only counterion present. Furthermore, the estimated macromolecule valences (111 charges/particle and 590 charges/particle for the 21- and 38-nm latexes, respectively) compare reasonably well with the manufacturer-quoted values of 130 and 680 charges/particle. The Ludox AM-30 colloidal silica dispersions were found to contain mainly Na^+ counterions with a negligible amount of H^+ and OH^- ions. The valence of these macromolecules was approximately 48 charges/particle. In all cases, the estimated macromolecule valences were found to be independent of the background electrolyte concentration at the ionic strengths used in the HFB experiments.

Mobilities of the macromolecules were measured at pH, electrolyte concentrations, and D_2O/H_2O ratios corresponding to the solutions used in the HFB experiments using the Brookhaven ZetaPlus electrophoresis instrument. Although the characterization was carried out on dilute suspensions, the change in ionic strength and/or pH due to dissociated counterions was accounted for by properly adjusting the concentrations of indifferent electrolyte and strong acid (HCl), respectively. Macromolecule zeta potentials were calculated from the mobility values using the mobility program of O'Brien and White (21).

For each suspension, the kinematic viscosity was determined with a Cannon-Fenske viscometer (Cole Parmer, Vernon Hills, IL) and converted to true viscosity using gravimetrically measured suspension densities. The results are summarized in Table 1. A temperature of $22^\circ C$ was maintained during both the HFB experiments and the characterization work.

Experimental Procedure

In performing the experiments, the microscope objective was focused in the fluid near the top plate where the latex particles would equilibrate. Because the particles and plate were negatively charged, the particles would reach a stable position where gravitational, electrostatic and depletion forces were balanced. Invariably, it was possible to find a small number of particles that had become adhered to the top plate. Locating these particles was performed by simply translating the bottom glass box and identifying particles that remained stationary against the shear flow.

Once a fixed particle was found, a doublet was produced by manipulating the bottom stage in order to collide a free particle with the stuck particle. At this point, the bottom plate was translated in a single direction at a constant velocity for several seconds. If the doublet did not separate, the velocity was increased slightly and the procedure repeated until separation was detected. This sequence was then repeated several times in opposite directions, as well as with other free particles. After that, a new stuck particle was located and the breakup tests performed again. The average separation velocity (and corresponding shear rate) was then computed, and the resulting separation force was determined using Eq. [19].

Analysis of Experimental Results

The total interaction between the two charged particles was assumed to be composed of an electrostatic repulsion, a van der Waals attraction, and a depletion interaction. Because charge effects were important in these experimental systems (i.e., the bulk Debye lengths were comparable to the size of the macromolecules), the interparticle depletion interaction was calculated using the force balance model originally developed by Walz and Sharma (16) and later advanced by Piech and Walz (22, 23). This model calculates the depletion interaction between two spherical particles immersed in a solution of nonadsorbing, charged macromolecules, such as that illustrated in Fig. 8. Performing a simple force balance to obtain the total force exerted on particle 1 by the surrounding macromolecules yields

$$F_1(h) = \int_{\mathbf{x}} \rho(\mathbf{x}) \nabla_1 E_1(\mathbf{x}) d\mathbf{x}, \quad [20]$$

where $\rho(\mathbf{x})$ is the number density of macromolecules at position \mathbf{x} and $\nabla_1 E_1(\mathbf{x})$ is the gradient of the interaction energy with respect to the surface of particle 1 (i.e., the interaction force exerted on particle 1 by the macromolecule).

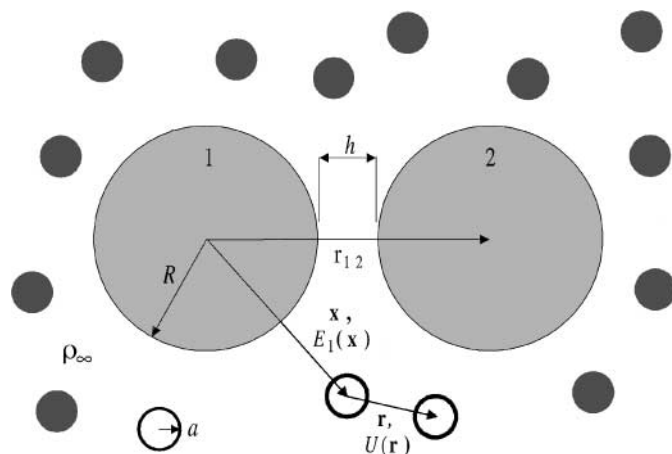


FIG. 8. This schematic depicts the system modeled in the force-balance approach of Walz and Sharma (16). Two charged, spherical particles of radius R are immersed in a solution of charged, spherical macromolecules of radius a and bulk number density ρ_∞ . The interaction energy between a single macromolecule and particle 1 is $E_1(\mathbf{x})$, while that between two macromolecules is $U(r)$.

In the limit of low macromolecule concentrations, the macromolecule distribution around the two particles will follow a Boltzmann distribution of the form

$$\rho(\mathbf{x}) = \rho_\infty \exp\left[\frac{-E(\mathbf{x})}{kT}\right], \quad [21]$$

where kT is the thermal energy and $E(\mathbf{x})$ represents the potential energy of mean force acting on the macromolecule at position \mathbf{x} . When two such particles, 1 and 2, are present, the resulting energy can be approximated as the sum of the two individual energies

$$E(\mathbf{x}) = E_1(\mathbf{x}) + E_2(\mathbf{x} - \mathbf{r}_{12}), \quad [22]$$

where \mathbf{r}_{12} is a vector that points from the center of particle 1 to the center of particle 2 (thus $\mathbf{x} - \mathbf{r}_{12}$ points from the center of particle 2 to a macromolecule located at position \mathbf{x}). Substituting equations [21] and [22] into [20] yields

$$\mathbf{F}_1(h) = \int_{\mathbf{x}} \rho_\infty \exp\left\{-\frac{[E_1(\mathbf{x}) + E_2(\mathbf{x} - \mathbf{r}_{12})]}{kT}\right\} \nabla_1 E_1(\mathbf{x}) d\mathbf{x}. \quad [23]$$

In more concentrated systems, interactions between the macromolecules themselves, even of the simple hard sphere type, will cause the equilibrium concentration of macromolecules in proximity to a surface to deviate from the Boltzmann distribution. Virial expansion of the density function is one method to take into account these macromolecule–macromolecule interactions. Specifically, for the case of a single macromolecule interacting simultaneously with two large particles plus another macromolecule, we can write

$$\rho(\mathbf{x}) = \rho_\infty \exp\left\{-\frac{[E_1(\mathbf{x}) + E_2(\mathbf{x} - \mathbf{r}_{12})]}{kT}\right\} \times \{1 + \rho_\infty[b_1(\mathbf{x}) + b_2(\mathbf{x} - \mathbf{r}_{12})] + O(\rho_\infty^2)\}, \quad [24]$$

where $b_1(\mathbf{x})$ and $b_2(\mathbf{x})$ are the second virial coefficients for a macromolecule at position \mathbf{x} interacting simultaneously with another macromolecule and the surface of particle 1 and particle 2, respectively. The virial coefficient for interactions with particles 1 and 2 were assumed additive here (valid for weak macromolecule–macromolecule interactions), and were calculated using (24)

$$b_k(\mathbf{x}') = \int_{\mathbf{r}} \left\{ \exp\left[-\frac{E_k(\mathbf{x}' + \mathbf{r})}{kT}\right] - 1 \right\} \times \left\{ \exp\left[-\frac{U(\mathbf{r})}{kT}\right] - 1 \right\} d\mathbf{r}, \quad [25]$$

where \mathbf{r} is the center-to-center distance between the two macromolecules, k is equal to either 1 ($\mathbf{x}' = \mathbf{x}$) or 2 ($\mathbf{x}' = \mathbf{x} - \mathbf{r}_{12}$),

and $U(\mathbf{r})$ is the macromolecule–macromolecule interaction energy (see Fig. 8). The expression for the depletion force in a monodisperse system is obtained by combining Eqs. [23] and [24], yielding

$$\mathbf{F}_1(h) = \int_{\mathbf{x}} \rho_\infty \exp\left\{-\frac{[E_1(\mathbf{x}) + E_2(\mathbf{x} - \mathbf{r}_{12})]}{kT}\right\} \times \{1 + \rho_\infty[b_1(\mathbf{x}) + b_2(\mathbf{x} - \mathbf{r}_{12})]\} \nabla_1 E_1(\mathbf{x}) d\mathbf{x}. \quad [26]$$

Piech and Walz later expanded this approach to consider systems in which the macromolecules were polydisperse (22) or spheroidal (23) in shape.

The terms $E(\mathbf{x})$ and $U(\mathbf{r})$ in the above equation represent the particle–macromolecule and macromolecule–macromolecule interaction energies, respectively. For the experiments described here, with charged spherical particles and macromolecules, the relevant electrostatic interaction energies were calculated using the linear superposition approach described by Bell *et al.* (25). This approach assumes that at any point between two spherical particles, the total potential can be approximated as the sum of the individual potentials, which is valid only for gap widths much larger than the bulk Debye length. The applicability of this particular approach for this problem is discussed in greater detail by Piech and Walz (22).

As discussed above, the presence of the nearby wall can only affect the interparticle interaction when the size of the particle is less than four times the effective size of the macromolecules. In the systems studied here, the particle radius was 4.8 μm , the largest macromolecule radius was 19 nm, and the largest Debye length was 15.4 nm (0.389 mM ionic strength). As discussed above, a rough estimate of the effective thickness of the charged double layer is $5\kappa^{-1}$. Using these values, the minimum ratio of the effective particle size to the effective macromolecule size in these experiments was 50, meaning that the effect of the wall could be ignored.

The purely electrostatic component of the interparticle interaction was calculated using the linear superposition approach of Bell *et al.* (25) described above. This model remains valid for large particles, provided that the interparticle gap width is much larger than the solution Debye length. We also considered whether the flat wall could have any impact on the interparticle electrostatic interaction. Sader and Chan (26) developed analytical expression for the electrostatic interaction between two particles next to a charged wall or confined between two charged walls. When the particle size was much greater than the bulk Debye length, which is easily satisfied in the present experiments, the wall effect was found to be unimportant.

Finally, the van der Waals contribution to the total interaction energy was calculated as

$$E_{\text{vdw}}(h) = -\frac{R}{12} \int_h^\infty \frac{A(\delta)}{\delta^2} d\delta, \quad [27]$$

where $A(\delta)$ is the Hamaker constant between two planar

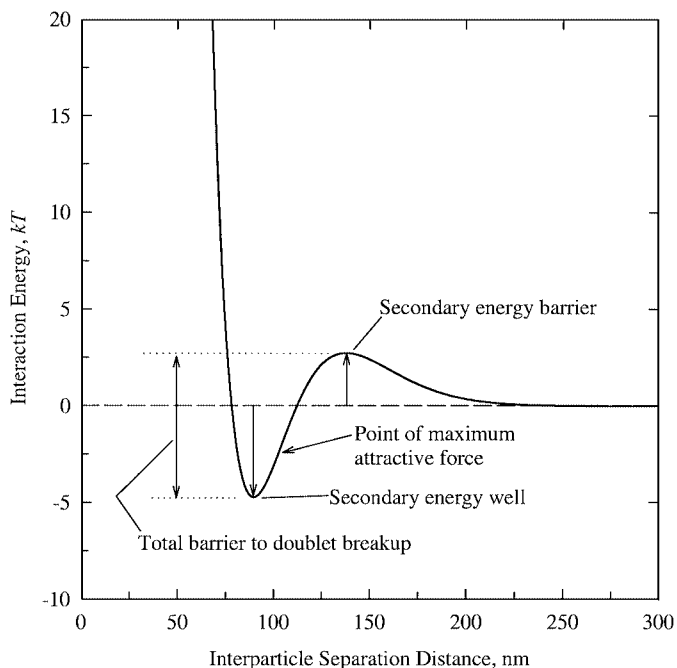


FIG. 9. This graph shows the model-predicted potential energy profile between two 9.6- μm -diameter latex particles. The total interaction energy was calculated as the sum of an electrostatic repulsion, a van der Waals attraction, and a depletion interaction. The total energy barrier to breakup of the doublet is the sum of the magnitudes of the secondary energy well and barrier. The specific parameters used here were those corresponding to the system in which 21-nm latex particles at a volume concentration of 0.50% were used as the macromolecules (see Table 1).

half-spaces separated by gap width δ , which was calculated using the Lifshitz continuum approach. The Derjaguin approximation has been applied in Eq. [27] to calculate the interaction energy between two spherical particles using the energy/area interaction between two half-spaces. The necessary spectroscopic data for polystyrene, glass, and water was taken from Parsegian and Weiss (27).

A typical interaction energy profile calculated in this manner is shown in Fig. 9. The conditions used for this curve were those corresponding to the experiment with 21-nm latex macromolecules at 0.50% vol. As seen, the energy profile is characterized by a significant secondary energy well at approximately 90 nm gap width. It is this energy well in which the particles become trapped when brought together at the start of an experiment (aggregation in the deeper, primary minimum would require much larger separation forces than those observed in these experiments). The energy profile also displays a longer-range energy barrier at approximately 130 nm. This secondary barrier, which has been predicted by numerous researchers (28–34), arises from an ordering of the small macromolecules in the gap region at higher bulk concentrations. In fact, the true interaction energy profile would have a decaying, oscillatory shape at large gaps, with the wavelength of the oscillations equal to the spacing between the macromolecule layers in the gap region. Because the Walz and Sharma model uses only a second-order

virial expansion, only the first barrier of this oscillatory structure is predicted.

The total energy barrier to separation of the doublet will be the sum of the magnitudes of the secondary barrier and secondary well. Between the secondary well and the secondary barrier, the slope of the profile goes through a maximum, which is where the attractive force between the two particles is greatest. Particle separation in the HFB experiments would thus occur when the magnitude of the viscous drag force (calculated using Eq. [19]) equals this maximum attraction.

RESULTS AND DISCUSSION

Comparison of Measured and Predicted Break Forces

The measured plate speeds at doublet breakup along with the corresponding shear rates and particle hydrodynamic forces, are given in Table 2. As can be seen, in a number of experiments, the doublet broke at all speeds. This was observed, for example, with each of the experiments using the 38-nm latex macromolecules. The values of plate speed given are actually averages over repeated experiments with the same particle pair (in two different directions), as well as different particle pairs. The standard deviations in plate speeds are also given, which were found to be as low as 4% of the mean in one case to as high as 32% of the mean in another.

A comparison between the measured and predicted particle separation forces is given in Table 3. Also listed here is the total energy barrier (in kT) holding the doublet together for each of the experimental systems. As seen, the predicted maximum force is found to be larger than the measured force in five of the six cases in which an interparticle attraction could be reliably measured. For several of the experiments, the predicted attraction force was below the sensitivity of the HFB technique (roughly estimated to be 10^{-13} N for these experiments). In only one case (21 nm latex, 0.25% vol.) was no attraction measured even though the predicted force was greater than this sensitivity limit.

For the experiments in which an attraction was measured, the average ratio of the predicted to the experimentally measured force needed for particle separation was 1.7. It should be emphasized that this comparison involves no adjustable parameters. In the discussion section, several factors that could possibly explain this discrepancy are presented.

There are two other issues that should be mentioned here. First, the hydrodynamic equations presented earlier assume laminar flow in the gap region. To validate this assumption, we calculated the Reynolds number for flow in the gap, defined here as

$$\text{Re} = \frac{Gd^2\rho}{\mu}, \quad [28]$$

where d is the plate spacing (approximately 120 μm in all experiments), ρ is the bulk density, and μ is the bulk viscosity. The maximum value of Re was 7×10^{-2} , indicating that the flow was laminar.

TABLE 2
The Measured Separation Velocity and Corresponding Shear Force for Each HFB Experiment

Macromolecule system	Effective ionic strength (mM)	Plate spacing (μm)	Plate speed at separation ^a ($\mu\text{m/s}$)	Shear rate at separation (s^{-1})	Separation force ^b (N)
12 nm Silica, 0.05% vol	0.406	123.9	—	—	—
12 nm Silica, 0.50% vol	0.607	118.4	133 ± 34	1.12 ± 0.29	$(6.79 \pm 1.74) \times 10^{-13}$
12 nm Silica, 0.50% vol	1.14	129.1	145 ± 20	1.12 ± 0.16	$(6.79 \pm 0.94) \times 10^{-13}$
12 nm Silica, 0.50% vol	1.67	120.0	46 ± 11	0.38 ± 0.09	$(2.20 \pm 0.53) \times 10^{-13}$
12 nm Silica, 0.80% vol	0.743	119.8	800 ^c	6.68	4.07×10^{-12}
21 nm Latex, 0.05% vol	0.413	125.7	—	—	—
21 nm Latex, 0.25% vol	0.447	122.9	—	—	—
21 nm Latex, 0.50% vol	0.522	134.3	135 ± 6	1.01 ± 0.04	$(5.98 \pm 0.24) \times 10^{-13}$
21 nm Latex, 0.68% vol	0.555	127.5	240 ± 50	1.88 ± 0.39	$(1.13 \pm 0.24) \times 10^{-12}$
38 nm Latex, 0.006% vol	0.395	124.3	—	—	—
38 nm Latex, 0.05% vol	0.389	141.5	—	—	—
38 nm Latex, 0.05% vol	1.46	128.9	—	—	—

^a No value indicates that the doublet separated at all velocities.

^b Calculated using Eq. [19].

^c Because of a problem with the motion control program, the actual separation speeds for this experiment could only be estimated. The true break speed is no lower than $800 \mu\text{m/s}$ and is believed to be only slightly larger than this, so a value of $800 \mu\text{m/s}$ was used to estimate the separation force.

The second issue was whether the concentration of macromolecules around the interacting particles could be affected by the shear flow. The relative importance of the flow (relative to Brownian movement of the macromolecules) can be characterized by the dimensionless Peclet number, Pe, defined as (35)

$$\text{Pe} = \frac{6\pi\mu a^3 G}{kT}. \quad [29]$$

For these experiments, the largest value of Pe was of order 10^{-5} , indicating that the viscous forces acting on the macromolecules

were much smaller than Brownian forces and thus the equilibrium distribution would be maintained.

Possible Causes of Discrepancy

We focus here on two possible causes of the discrepancy: the size and size distribution of the macromolecules, and the stochastic nature of the doublet breakup process. Although there are clearly several other potential areas of uncertainty in the measured parameters (e.g., the zeta potentials of the particles and macromolecules), these two effects are thought to be the largest contributors to deviations from the predicted results.

TABLE 3
Comparison of the Measured and Predicted Particle Separation Forces

Macromolecule system	Effective ionic strength (mM)	Predicted energy profile		Measured separation force (N)	Maximum attractive force/measured separation force
		Total barrier to particle separation (kT)	Maximum attractive force (N)		
12 nm Silica, 0.05% vol	0.406	0.063	1.95×10^{-15}	—	—
12 nm Silica, 0.50% vol	0.607	9.30	2.15×10^{-12}	$(6.79 \pm 1.74) \times 10^{-13}$	3.17
12 nm Silica, 0.50% vol	1.14	1.55	5.42×10^{-13}	$(6.79 \pm 0.94) \times 10^{-13}$	0.80
12 nm Silica, 0.50% vol	1.67	1.32	3.27×10^{-13}	$(2.20 \pm 0.53) \times 10^{-13}$	1.49
12 nm Silica, 0.80% vol	0.743	27.84	6.08×10^{-12}	4.07×10^{-12}	1.49
21 nm Latex, 0.05% vol	0.413	0.11	5.81×10^{-15}	—	—
21 nm Latex, 0.25% vol	0.447	2.13	3.02×10^{-13}	—	—
21 nm Latex, 0.50% vol	0.522	7.43	1.08×10^{-12}	$(5.98 \pm 0.24) \times 10^{-13}$	1.81
21 nm Latex, 0.68% vol	0.555	11.65	1.71×10^{-12}	$(1.13 \pm 0.24) \times 10^{-12}$	1.51
38 nm Latex, 0.006% vol	0.395	0.051	1.67×10^{-15}	—	—
38 nm Latex, 0.05% vol	0.389	0.13	7.40×10^{-15}	—	—
38 nm Latex, 0.05% vol	1.46	0.57	4.33×10^{-14}	—	—

Avg. = 1.71

Size and size distribution of the macromolecules. Both the silica and the polystyrene particles used as the macromolecules in these experiments were polydisperse. For example, the manufacturer of the 21-nm latex particles, Interfacial Dynamics Corporation, quoted a coefficient of variation of 14.8% (corresponding to a standard deviation of 3.83 nm) for the particle size distribution. Recently, Piech and Walz (22) modified the model of Walz and Sharma to account for a distribution in either the size or surface potential of the nonadsorbing macromolecules. A log-normal distribution, characterized by a mean and standard deviation, was assumed. Using this model, we recalculated the potential energy profile and the resulting maximum attractive force for the experimental systems used here.

The effect of polydispersity on the potential energy profile can be seen in the graph shown in Fig. 10, which was calculated using the conditions of the experiment with 21-nm latex macromolecules at 0.50% vol. In performing these calculations, we assumed that the total volume fraction of macromolecules remained fixed, which is consistent with the approach used to prepare the solutions in which a specific weight of particles (corresponding to a specific volume of particles) was measured. As can be seen in the figure, the polydispersity lowers both the height of the secondary barrier and the depth of the secondary well, which results in a reduction in the maximum attractive force by 13%. These smaller energy wells result from the fact that the number density of macromolecules must be lower in the polydisperse

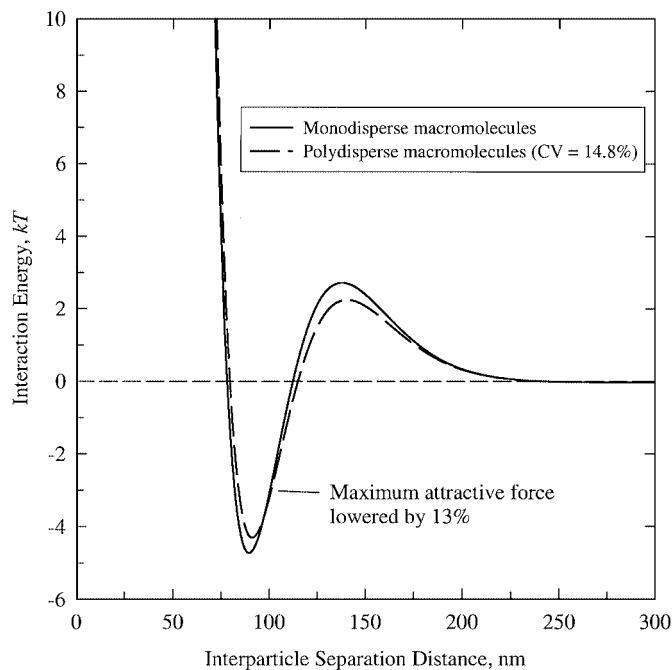


FIG. 10. This graph shows the effect of polydispersity in the macromolecule size on the depletion interaction. The experimental system is that using 21-nm latex particles at 0.50 vol% (see Table 1). The polydispersity effect was calculated using the modified Walz and Sharma model described by Piech and Walz (22). The magnitude of the polydispersity (standard deviation/mean of 14.8%) was provided by the manufacturer (Interfacial Dynamics Corporation).

case in order to maintain the same volume fraction, which is the dominant effect on the depletion interaction. (The only exception is the system using 0.05% vol. macromolecules, where the weak attraction is caused primarily by van der Waals forces.)

The change in the maximum attractive force for each of the 21-nm latex macromolecule systems is given in the top half of Table 4. As seen, with the exception of the 0.05% vol. macromolecule case, the predicted separation force is reduced, providing better agreement with the measured force. Specifically, the ratio of the predicted-to-measured force drops from an average of 1.7 to 1.2 for these systems.

Unfortunately, the size distribution for the Ludox silica particles was not known, as no value was reported by the manufacturer and attempts to measure the sizes using transmission electron microscopy were unsuccessful. However, a more important issue may be the actual macromolecule size. Specifically, the size of 12 nm used in the calculations presented above was taken from a data sheet on Ludox colloidal silica obtained from Dupont (the actual manufacturer of the silica particles). However, published measurements of the dry diameter of Ludox HS particles, also listed as 12 nm in diameter on the Dupont data sheet, range from 13.5 to over 19 nm (36–39). Another possible factor is the presence of particle aggregates, which were observed using similar Ludox AM particles by Matijević *et al.* (40).

To determine the effect of uncertainty in the macromolecule size, we performed a series of model runs using a conservative value of 14 nm as the diameter of the macromolecules. Again, since the solutions were prepared using a targeted weight of silica particles, the volume fraction of particles was kept fixed, meaning that the number density of macromolecules was decreased. The results of these calculations are shown in the bottom half of Table 4. As seen, in most of the cases, the predicted separation force was decreased. The nature of the change in the maximum attractive force is determined by a balance between the effects of a lower macromolecule number density and a larger excluded volume around the particle. Each of these effects varies nonlinearly with macromolecule size. Overall, the average ratio of the predicted-to-measured separation forces decreases from 1.7 to 1.4.

In summary, it is clear that a significant part of the discrepancy between the predicted and measured separation forces can be explained by either the known polydispersity or uncertainties in the actual diameter of the macromolecules. In the following section, we review one other possible source of error, namely the stochastic nature of the doublet breakup process.

Stochastic nature of breakup process. In the above analysis, separation of the doublet was assumed to occur when the shear force acting on the free particle was equal to the maximum attractive force. Ignored in this analysis, however, is the fact that the free particle is Brownian and thus the actual breakup process is stochastic. A more relevant method for analyzing the results would thus be to calculate how the shear force alters the interparticle potential energy profile, such as that shown in Fig. 9.

TABLE 4
Effect of Polydispersity and Macromolecule Size on the Predicted Separation Force

Macromolecule concentration (% vol)	Effective ionic strength (mM)	Measured separation force (N)	Predicted separation force with no polydispersity (N)	Predicted separation force with 14.8% polydispersity (N)
21-nm Polystyrene systems				
0.05	0.413	—	5.81×10^{-15}	5.97×10^{-15}
0.25	0.447	—	3.02×10^{-13}	2.66×10^{-13}
0.50	0.522	$(5.98 \pm 0.24) \times 10^{-13}$	1.08×10^{-12}	9.36×10^{-13}
0.68	0.555	$(1.13 \pm 0.24) \times 10^{-12}$	1.71×10^{-12}	1.48×10^{-12}
		Avg. predicted/measured ratio	1.66	1.23
			Predicted separation force with 12 nm macromolecule diameter	Predicted separation force with 14 nm macromolecule diameter
Ludox silica systems				
0.05	0.406	—	1.95×10^{-15}	2.26×10^{-15}
0.50	0.607	$(6.79 \pm 1.74) \times 10^{-13}$	2.15×10^{-12}	1.40×10^{-12}
0.50	1.14	$(6.79 \pm 0.94) \times 10^{-13}$	5.42×10^{-13}	5.13×10^{-13}
0.50	1.67	$(2.20 \pm 0.53) \times 10^{-13}$	3.27×10^{-13}	3.68×10^{-13}
0.80	0.743	4.07×10^{-12}	6.08×10^{-12}	3.78×10^{-12}
		Avg. predicted/measured ratio	1.73	1.35

In the presence of a constant shear force, the total potential energy of the free particle can be written as

$$E(h) = E_{\text{dep}}(h) + E_{\text{elect}}(h) + E_{\text{vdw}}(h) + E_{\text{shear}}(h), \quad [30]$$

where $E_{\text{shear}}(h)$ will be equal to the shear force, given by Eq. [19], times the gap width, h . Thus

$$E_{\text{shear}}(h) = 1.17(6\pi)\mu GR^2h. \quad [31]$$

This equation assumes that the shear force is relatively constant with distance over the range of interest. Shown in Fig. 11 are three potential energy curves demonstrating the effect of a constant shear force. The solid line is the potential energy profile calculated with no shear force included for the experimental system using 21-nm latex macromolecules at 0.50% vol. Polydispersity in the size of the macromolecules ($CV = 14.8\%$) has been included. For the dashed line, the shear force was set equal to the predicted maximum attractive force (9.36×10^{-13} N) given in Table 4. As seen, at this critical shear force, the magnitude of the total energy barrier to breakup of the doublet is exactly zero.

By comparison, for the broken (dash-dot-dot) line, the shear component was calculated using the measured separation force (5.98×10^{-13} N). As seen, an energy well is still present, however the total depth of this well is only approximately $1.3 kT$, meaning that probability of particle detachment would be relatively high. Moreover, because the potential energy drops rapidly beyond this well, detachment would be essentially irreversible.

In addition to the depth of the energy well, the time required for the particle to escape is also important since escape can occur

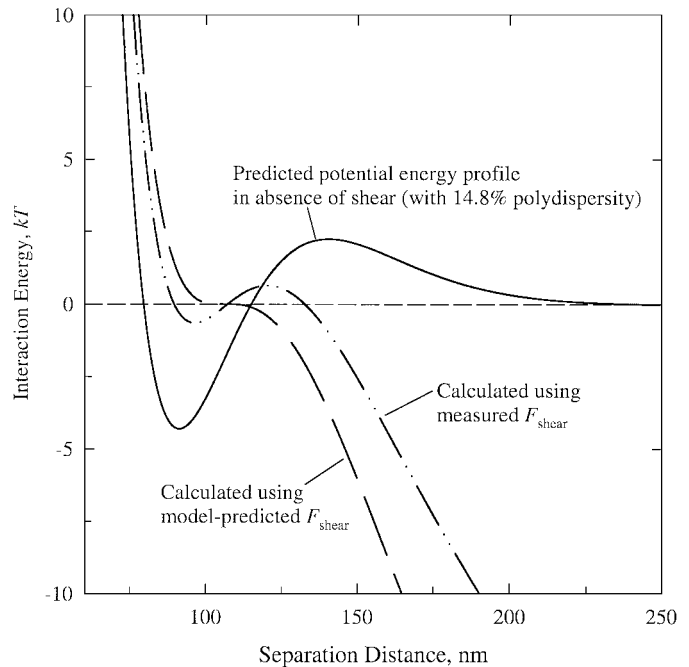


FIG. 11. This graph shows the effect of a constant shear force on the total interparticle potential energy profile. These calculations were performed using the parameters corresponding to the experiment with 21-nm latex particles at 0.50 vol% (see Table 1), along with 14.8% polydispersity in the size of the macromolecules. The solid curve gives the energy profile calculated without shear. For the dashed curve, the shear force was set equal to the maximum predicted attractive force between the particles (9.36×10^{-13} N here). The shear component of the energy was calculated as the shear force times the separation distance. For the broken (dash-dot-dot) line, the shear force was the actual measured force obtained from the HFB experiments (5.98×10^{-13} N here). As seen, using the measured separation force, an energy barrier to breakup of the doublet of approximately $1.3 kT$ is predicted.

only if this time is smaller than the length of the experiment. To calculate this time, a series of Brownian dynamics simulations was performed using the method of Clark *et al.* (41). For one-dimensional Brownian motion, the displacement of the free particle, Δh , in time Δt can be calculated as

$$\Delta h = \frac{D}{kT} F \Delta t + \frac{\partial D}{\partial h} \Delta t + \chi \sqrt{2D \Delta t}, \quad [32]$$

where D is the particle's diffusion coefficient at position h , F is the net force acting on the particle at position h , and χ is randomly chosen from a series of normally distributed numbers with a mean of zero and a standard deviation equal to one. The first term on the rhs of Eq. [32], referred to as the drift term, is the change in position due to external forces. The second term accounts for any spatial dependence of the diffusion coefficient and tends to move the particle in the direction of higher mobility, and the third term is the stochastic contribution to the change in position.

The diffusion coefficient of the free particle can be calculated as kT/f , where f is the friction coefficient for particle motion along the line of centers between two neighboring particles next to a solid wall. The total friction factor for this system can be calculated as $f_1 + f_2$, where f_1 is the resistance to motion of a single particle parallel to a solid wall and f_2 is the resistance to motion along the line of centers between two hard particles. The resistance for motion of a particle parallel to a solid wall was given by Goldman *et al.* (42) as

$$f_1 = 6\pi\mu R \left(\frac{8}{15} \ln(R/h') + 0.9588 \right), \quad [33]$$

where h' is the particle–plate gap width. An expression for the resistance between two spherical particles moving along their line of centers was given by van de Ven (43) in the form of an infinite series. The following simple approximation of this function, found to be accurate to within a few percent, was given by Honig *et al.* (44),

$$f_2 = 6\pi\mu R \left(\frac{6\hat{h}^2 + 13\hat{h} + 2}{6\hat{h}^2 + 4\hat{h}} \right), \quad [34]$$

where \hat{h} is the particle–particle gap width, h , divided by the particle radius, R .

The time step, Δt , in Eq. [32] must satisfy two requirements. First, Δt must be larger than the momentum relaxation time for Brownian fluctuations, and second, Δt must be small enough that the diffusion coefficient remains relatively constant during a change in position Δh . The Brownian relaxation time is of order $m/6\pi\mu R$, where m is the particle mass (41). For a 10- μm diameter polystyrene sphere, this time is approximately 5×10^{-6} s. Thus for these simulations Δt was set to 10^{-4} s. We

found that the typical change in position, Δh , during this time step led to negligible changes in the diffusion coefficient.

To perform these calculations, the force profile acting between the particles was calculated using the measured separation force (i.e., the force profile corresponding to the dash-dot-dot energy profile in Fig. 11). The initial position of the particle was set to 96 nm, which is the position of the secondary energy minimum. For calculation purposes, the particle–wall separation distance, h' , was also set to 96 nm (this distance remained fixed in the simulation). Note that because the particle–particle resistance, f_2 , is the dominant resistance, using different values of h' had little effect on the final results. The simulation then proceeded through a series of time steps and the change in position during each step, Δh , was calculated using Eq. [32]. The new position of the particle was calculated at the end of each step as $h_{\text{new}} = h_{\text{old}} + \Delta h$, and this new position was used in the following time step. The program was run until the particle–plate separation, h , reached a value of 1 μm , corresponding to the estimated distance needed to detect separation in the HFB experiments. A total of 10,000 such simulations were run and the average time needed for doublet separation was found to be 2.1 s. Since each shear flow was applied for at least several seconds in the HFB experiments, the free particle would, on average, have more than enough time to diffuse over the small energy barrier present at the measured separation force.

In summary, the stochastic nature of the particles means that breakup of the doublet would be likely at the measured separation forces. Table 5 lists the magnitude of the resulting energy barriers to doublet breakup calculated using the measured separation forces for the other experimental systems in which a measurable attraction was found. For these calculations, the Ludox diameter was assumed to be 14 nm and the known polydispersity in the size of the 21 nm latex particles was included. As seen, the largest energy barrier was approximately 2.3 kT , which would not significantly inhibit separation. For example, Feigin and Napper (45) suggest that energy barriers of at least 15–20 kT are necessary to prevent rapid flocculation of bulk particles.

TABLE 5
Predicted Energy Wells at the Measured Separation Force

Macromolecule system, (% vol)	Effective ionic strength (mM)	Predicted energy barrier in the absence of shear (kT)	Predicted energy barrier at the measured separation force (kT)
12 nm Silica, 0.50% vol ^a	0.607	6.53	2.27
12 nm Silica, 0.50% vol ^a	1.14	1.87	No barrier
12 nm Silica, 0.50% vol ^a	1.67	1.79	0.27
12 nm Silica, 0.80% vol ^a	0.743	18.04	No barrier
21 nm Latex, 0.50% vol ^b	0.522	6.54	1.29
21 nm Latex, 0.68% vol ^b	0.555	10.18	1.05

^a Assuming 14 nm macromolecule diameter.

^b Including 14.8% polydispersity in the size of the macromolecules.

SUMMARY

A relatively simple expression was derived for calculating the effect of a solid, neighboring wall on the depletion interaction between two particles. Both particles are assumed to be identical and located equidistant from the wall. Although not explicitly given here, this same expression could be used to determine how the interaction between a single particle and wall is affected by a neighboring particle. A useful finding from this analysis is that the equations describing the bulk interparticle interaction (i.e., the Asakura and Oosawa potential) remain valid at all particle-wall separations as long as the ratio of the particle radius to the macromolecule radius is greater than four, a criterion that is satisfied in many experimental systems.

Depletion forces as low as 2×10^{-13} N were measured between two 10- μ m diameter particles in a solution of small, negatively charged nanospheres using the hydrodynamic force balance (HFB) apparatus. Because of the large particle-to-macromolecule size ratios, wall effects were insignificant in these experiments. It was found that the maximum attractive force holding a doublet together in a secondary energy well could be predicted relatively accurately with the force balance model of Walz and Sharma (16), which was developed to study depletion interactions with charged particles and macromolecules, without any adjustable parameters. Specifically, when the effects of polydispersity and variability in the macromolecule size were included, the average ratio of the predicted-to-measured separation force was 1.3. It was shown that this remaining discrepancy could easily be explained by the Brownian, or stochastic, nature of the doublet breakup process.

It should be mentioned that one experimental system that could be used to explicitly probe the effects of a wall on the interparticle depletion interaction is one in which the depletion force is produced by long, thin rods. In such a system, the characteristic length scale of the depletion interaction is the rod length (46), which can be made quite large with the total volume fraction of rods remaining small, provided the rods are sufficiently thin (i.e., very high aspect ratios). A possible material would be bacteriophage fd virus used by Adams *et al.* (47), which has a counter length of 880 nm and a diameter of 6.6 nm.

ACKNOWLEDGMENTS

Financial support for this work was provided by the National Science Foundation through Grant CTS-970277. J.Y.W. also personally thanks Dr. Jan Czarniecki of Syncrude Canada Ltd. for assisting in the arrangement of his visit to Syncrude's Edmonton Research Centre.

REFERENCES

- Asakura, S., and Oosawa, F., *J. Chem. Phys.* **22**, 1255 (1954).
- Asakura, S., and Oosawa, F., *J. Polym. Sci.* **33**, 183 (1958).
- De Hek, H., and Vrij, A., *J. Colloid Interface Sci.* **70**, 592 (1979).
- De Hek, H., and Vrij, A., *J. Colloid Interface Sci.* **84**, 409 (1981).
- Sperry, P. R., Hopfenberg, H. B., and Thomas, N. L., *J. Colloid Interface Sci.* **82**, 62 (1981).
- Sharma, A., Tan, S., and Walz, J. Y., *J. Colloid Interface Sci.* **191**, 236 (1997).
- Promislow, J. H. E., "Structural Evolution in Magnetorheological Fluids: Kinetics and Energetics," Ph.D. thesis, Stanford University, 1997.
- Rosenbaum, D. F., and Zukoski, C. F., *J. Crystal Growth* **169**, 752 (1996).
- Kulkarni, A. M., Chatterjee, A. P., Schweizer, K. S., and Zukoski, C. F., *Phys. Rev. Lett.* **83**, 4554 (1999).
- Kulkarni, A. M., Chatterjee, A. P., Schweizer, K. S., and Zukoski, C. F., *J. Chem. Phys.* **113**, 9863 (2000).
- De Kruijff, C. G., in "Food Emulsions and Foams: Interfaces, Interactions and Stability" (E. Dickinson and J. M. R. Patino, Eds.), pp. 29–44, Royal Society of Chemistry, Cambridge, 1999.
- Dinsmore, A. D., Yodh, A. G., and Pine, D. J., *Nature* **383**, 239 (1996).
- Dinsmore, A. D., Warren, P. B., Poon, W. C. K., and Yodh, A. G., *Europhys. Lett.* **40**, 337 (1997).
- Dinsmore, A. D., Wong, D. T., Nelson, P., and Yodh, A. G., *Phys. Rev. Lett.* **80**, 409 (1998).
- Dinsmore, A. D., and Yodh, A. G., *Langmuir* **15**, 314 (1999).
- Walz, J. Y., and Sharma, A., *J. Colloid Interface Sci.* **168**, 485 (1994).
- Piech, M., and Walz, J. Y., *Langmuir* **16**, 7895 (2000).
- Odiachi, P. C., and Prieve, D. C., *Colloids Surf., A* **146**, 315 (1999).
- Wu, X., Dabros, T., and Czarniecki, J., *Langmuir* **15**, 8706 (1999).
- Dabros, T., and van de Ven, T. G. M., *J. Colloid Interface Sci.* **149**, 493 (1992).
- O'Brien, R. W., and White, L. R., *J. Chem. Soc. Faraday Trans. 2* **74**, 1607 (1978).
- Piech, M., and Walz, J. Y., *J. Colloid Interface Sci.* **225**, 134 (2000).
- Piech, M., and Walz, J. Y., *J. Colloid Interface Sci.* **232**, 86 (2000).
- Glandt, E. D., *J. Colloid Interface Sci.* **77**, 512 (1980).
- Bell, G. M., Levine, S., and McCartney, L. N., *J. Colloid Interface Sci.* **33**, 335 (1970).
- Sader, J. E., and Chan, D. Y. C., *J. Colloid Interface Sci.* **218**, 423 (1999).
- Parsegian, V. A., and Weiss, G. H., *J. Colloid Interface Sci.* **81**, 285 (1981).
- Henderson, D., *J. Colloid Interface Sci.* **121**, 486 (1988).
- Yethiraj, A., Hall, C. K., and Dickman, R., *J. Colloid Interface Sci.* **151**, 102 (1992).
- Mao, Y., Cates, M. E., and Lekkerkerker, H. N. W., *Physica A* **222**, 10 (1995).
- Dickman, R., Attard, P., and Simonian, V., *J. Chem. Phys.* **107**, 205 (1997).
- Götzelmann, B., Evans, R., and Dietrich, S., *Phys. Rev. E* **57**, 6785 (1998).
- Tehver, R., Maritan, A., Koplik, J., and Banavar, J. R., *Phys. Rev. E* **59**, R1339 (1999).
- Roth, R., Evans, R., and Dietrich, S., *Phys. Rev. E* **62**, 5360 (2000).
- Russel, W. B., Saville, D. A., and Schowalter, W. R., "Colloidal Dispersions," Cambridge Univ. Press, Cambridge, 1989.
- Dezelic, G., Wrisher, M., Devide, Z., and Kratochvil, J. P., *Kolloid Z.* **171**, 42 (1960).
- Depasse, J., and Watillon, A., *J. Colloid Interface Sci.* **33**, 430 (1970).
- Iler, R. K., in "Surface and Colloid Science" (E. Matijević, Ed.), Vol. 6, p. 1. Wiley-Interscience, New York, 1973.
- Ramsay, J. D. F., Avery, R. G., and Benest, L., *Faraday Discuss. Chem. Soc.* **76**, 53 (1983).
- Matijević, E., Mangravite, F. J., and Cassell, E. A., *J. Colloid Interface Sci.* **35**, 560 (1971).
- Clark, A. T., Lal, M., and Watson, G. M., *Faraday Discuss. Chem. Soc.* **83**, 179 (1987).
- Goldman, A. J., Cox, R. G., and Brenner, H., *Chem. Eng. Sci.* **22**, 637 (1967).
- Van de Ven, T. G. M., "Colloidal Hydrodynamics," Academic Press, London, 1989.
- Honig, E. O., Roeberson, G. J., and Wiersema, P. H., *J. Colloid Interface Sci.* **36**, 97 (1971).
- Feigin, R. I., and Napper, D. H., *J. Colloid Interface Sci.* **75**, 525 (1980).
- Koenderink, G. H., Vliegthart, G. A., Kluijtmans, S. G. J. M., van Blaaderen, A., Philipse, A. P., and Lekkerkerker, H. N. W., *Langmuir* **15**, 4693 (1999).
- Adams, M., Dogic, Z., Keller, S. L., and Fraden, S., *Nature* **393**, 349 (1998).